Geomechanics and Engineering, *Vol. 17, No. 4 (2019) 343-354*
DOI: https://doi.org/10.12989/gae.2019.17.4.343

Impact of pore fluid heterogeneities on angle-dependent reflectivity in poroelastic layers: A study driven by seismic petrophysics

Mubasher Ahmad[1a], Nisar Ahmed[*1], Perveiz Khalid[1c], Muhammad A. Badar[1a], Sohail Akram[1c], Mureed Hussain[2c], Muhammad A. Anwar[1a], Azhar Mahmood[3d], Shahid Ali[1b] and Anees U. Rehman[4a]

[1]*Institute of Geology, University of the Punjab, Lahore 54590, Pakistan*
[2]*Department of Marine Geology, Lasbela University of Agriculture, Water and Marine Sciences, Uthal, Lasbela, Pakistan*
[3]*Petrophysics, Software Integrated Solution (SIS) Data Services Schlumberger, Pakistan*
[4]*Department of Earth Sciences, Quaid-I-Azam University, Islamabad, Pakistan*

(Received September 27, 2017, Revised January 9, 2019, Accepted February 22, 2019)

Abstract. The present study demonstrates the application of seismic petrophysics and amplitude versus angle (AVA) forward modeling to identify the reservoir fluids, discriminate their saturation levels and natural gas composition. Two case studies of the Lumshiwal Formation (mainly sandstone) of the Lower Cretaceous age have been studied from the Kohat Sub-basin and the Middle Indus Basin of Pakistan. The conventional angle-dependent reflection amplitudes such as P converted P (R_{PP}) and S (R_{PS}), S converted S (R_{SS}) and P (R_{SP}) and newly developed AVA attributes (ΔR_{PP}, ΔR_{PS}, ΔR_{SS} and ΔR_{SP}) are analyzed at different gas saturation levels in the reservoir rock. These attributes are generated by taking the differences between the water wet reflection coefficient and the reflection coefficient at unknown gas saturation. Intercept (A) and gradient (B) attributes are also computed and cross-plotted at different gas compositions and gas/water scenarios to define the AVO class of reservoir sands. The numerical simulation reveals that ΔR_{PP}, ΔR_{PS}, ΔR_{SS} and ΔR_{SP} are good indicators and able to distinguish low and high gas saturation with a high level of confidence as compared to conventional reflection amplitudes such as P-P, P-S, S-S and S-P. In A-B cross-plots, the gas lines move towards the fluid (wet) lines as the proportion of heavier gases increase in the Lumshiwal Sands. Because of the upper contacts with different sedimentary rocks (Shale/Limestone) in both wells, the same reservoir sand exhibits different response similar to AVO classes like class I and class IV. This study will help to analyze gas sands by using amplitude based attributes as direct gas indicators in further gas drilling wells in clastic successions.

Keywords: AVO modeling; fluid moduli; Indus basin; Zoeppritz equations; intercept-gradient; rock physics

1. Introduction

The amplitude variation with incident angle (AVA) describes the reflectivity of P and S incident waves at reservoir interface as a function of incident angles and this technique is a key component in a rising number of geophysical research campaigns. AVA analysis of seismic data is extensively used to predict hydrocarbons (especially natural gas) bearing sediments and characterizes the subsurface materials properties (Booth *et al.* 2016). Thus, the efficacy of AVA modeling and common linearized inversion algorithms to guesstimate the hydrocarbons saturation levels and quality from pre-stack seismic data or geophysical well logs depends on the difference in compressional and shear wave velocities and bulk density across the reservoir interface (Ahmed *et al.* 2015). The set of Zoeppritz equations (1919) provide fundamental basis to depict the reflection amplitudes variations as a function of incident angles and seismic parameters like seismic wave velocities and density of both upper and lower geological interfaces. However, the exact Zoeppritz equations are in the form of complex matrices and require more than 80 mathematical steps to solve them into linear forms for P and S waves reflection coefficients (Zhi *et al.* 2016). In the past five decades, a series of linearized mathematical forms of the Zoeppritz equations have been derived. Khan *et al.* (2015) and Ahmed *et al.* (2017a) have discussed the detail of various kinds of linear equations of P and S wave reflection amplitudes.

Observation of the variation in P-P, P-S, S-S and S-P seismic reflectivities with respect to incident angles or offset is successfully used to differentiate water/gas saturated sands. However, the sensitivity of the conventional particle displacement reflection coefficients (R_{PP}, R_{PS}, R_{SS} and R_{SP}) to partially gas saturated rocks is a subject of hot discussion (Zhu *et al.* 2000, Khalid *et al*. 2014, Ahmed *et al.* 2016, Khalid and Ahmed 2016). Therefore, various authors derived the modified forms of P and S wave reflection coefficients. Gomez and Tatham (2007) calculated the sensitivity of seismic reflectivity for fully and partially gas saturated reservoirs by taking partial and full derivatives of R_{PP}, R_{PS} and R_{SS}. Zhu *et al.* (2000) gave the concept of $\Delta R_{PP}/\Delta R_{PS}$ and $\Delta R_{PS}/\Delta R_{PP}$ and determined these attributes by taking difference between

*Corresponding author, Lecturer
E-mail: ahmedseis23@gmail.com
[a]M. Phil. Research Scholar
[b]Lecturer
[c]Assistant Professor
[d]Petrophysicist

http://www.techno-press.org/?journal=gae&subpage=7
ISSN: 2005-307X (Print), 2092-6219 (Online)

reflection coefficients computed in a fully water saturated zone and another target zone with unknown saturation. All these reflection coefficients are strongly influenced by fundamental seismic parameters (V_P, V_S and ρ).

Various AVO based attributes including intercept and gradient crossplotting (Shuey 1985), fluid factor (Smith and Gidlow 1987), pore space modulus (Hedlin 2000) etc. have been intensively used in the industry. Silin and Goloshubin (2010) developed asymptotic equation for seismic modeling and frequency dependent attribute (normal incident reflection amplitude) analysis within seismic frequency band (1-100 Hz). They have used a dimensionless parameter ε by considering signal frequency, fluid density and inverse of fluid viscosity. Asymptotic expression numerically calculates the normal incidence reflection coefficient at low seismic frequency and effectively applicable to discriminate gas bearing reservoirs from water bearing reservoirs (Xu *et al.* 2011). Many geophysicists (Chapman *et al.* 2006, Innanen 2012, Wu *et al.* 2014, Zhao *et al*. 2015; Zhang *et al*. 2016) have studied numerically the effect of velocity dispersion and attenuation on frequency-dependent amplitude variation with angle (AVAF) and perceived that AVAF behavior is more closely comparable to the true AVO response. Recently, Liu *et al.* (2019) presented a new fluid factor attribute as hydrocarbon indicator in the sedimentary sequence and verified it through stochastic Monte Carlo modeling.

To estimate the seismic parameters of saturated or partially saturated porous media with high level of confidence, the elastic properties of fluid saturated rocks and seismic petrophysics analysis is opted (Narongsirikul *et al.* 2019). Seismic petrophysics shows how quantitative seismic interpretation can be made more simple and robust by integrating the rock physics principles with seismic and petrophysical attributes (Golikov *et al.* 2013).

It can be effectively useful to find out seismic properties of saturated rock as a function of pore fluid's type, saturation and nature. The studies performed by Batzle and Wang (1992) on seismic and elastic properties of pore fluids illustrated that these properties are strongly affected by physical properties of hydrocarbon fluids such as specific gravity, viscosity, molecular weight and in-situ temperature-pressure.

In this study, P converted P and S reflection amplitudes and S converted S and P reflection amplitudes as function of incident angles are computed and plotted at different gas saturation levels for two different cases (I and II) of Lower Cretaceous reservoir from Indus Basin of Pakistan. This paper also discuss how ΔR_{PP}, ΔR_{PS}, ΔR_{SS} and ΔR_{SP} might be better gas indicators when conventional AVA based reflection coefficients failed to distinguish gas zones. AVA classes for Lumshiwal Sandstones are defined by extracting and crossplotting intercept and gradient for both cases. Intercept-gradient response at the top gas sands is also modeled at different compositions of natural gas. Seismic and elastic properties of fluids (gas/brine) and saturated rock are estimated by using fluid substitution and rock physics models.

2. Geological setting

Tectonically, Pakistan can be categorized into three main sedimentary basins of which the Indus Basin (IB) is the largest and the only oil and gas producing basin. The IB is further classified into the Upper (also called Kohat-Potwar Sub-basins) and the Lower (sub-divided into central and southern) Indus Basins (Kadri 1995). In the Kohat-Potwar area, the sedimentation started in the Precambrian and continued until the Pleistocene. The Salt Range Formation is the oldest sedimentary rock overlain metamorphic rocks in the Kohat-Potwar area. The three main unconformities in the area are Eocene to Oligocene, Mesozoic to late Permian and Ordovician to Carboniferous. In the Lower Indus Basin (LIB), the formation of horst-graben structures and tilted fault blocks are resulted due to rifting and parting of the Indian plate (IP) from the Gondwana and these structures are favorable for hydrocarbon accumulation. Sedimentary successions in the LIB began from carbonates of Triassic and proceed to recent alluvium (Baig *et al.* 2016). Middle part of IB comprises of the Punjab Platform, the Sulaiman Depression and the Sulaiman Fold Belt. Fig. 1 portrays all the sedimentary basins of the Pakistan including the Indus Basin and its division.

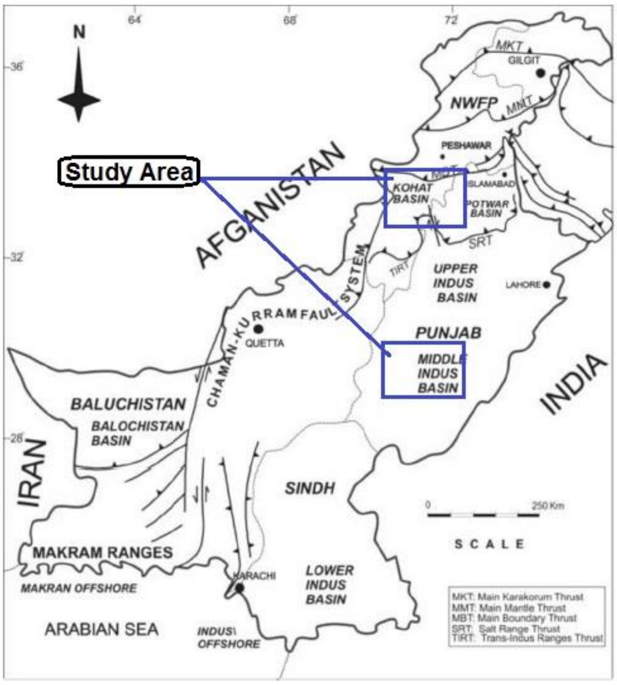

Fig. 1 Tectonic map of Pakistan, showing the Indus Basin and its subdivision into Upper, Middle, Lower parts. Other basins like the Baluchistan and the Peshawar Basins are also mentioned in the figure. Study areas are highlighted with boxes (blue color) that lie in the Upper and the Middle Indus Basins (Modified after Kazmi and Rana 1982)

The Lower Cretaceous Lumshiwal Formation is the reservoir rock in the study area that is widely exposed in the Upper Indus Basin and present in subsurface in the Central Indus Basin. It is mainly comprised of thick bedded to massive, medium to coarse grained, current bedded and cemented sandstone with the inclusion of silty, sandy, glauconitic shale inferring the cyclic alternation towards the transitional phase with the Chichali Formation. Two case studies of the Lower Cretaceous Lumshiwal Formation from the Kohat Sub-basin and the Central Indus Basin

(Punjab Platform) have considered for this research and also highlighted in Fig. 1. In case I, the Lumshiwal Formation (Sandstone) has upper contact with the Early Paleocene Khadro Formation (shale), a member of Ranikot Group and in case II, it has upper contact with the Lower Cretaceous Darsamand Limestone.

3. Methods and data used

Wireline logs data of two wells (case I and case II) drilled in the study area (one well from the Kohat Sub-basin and other is from the Middle Indus Basin) consists of gamma ray, resistivity, self-potential, induction, bulk density, neutron-porosity and sonic transit time logs etc. Formation tops data, reservoir temperature and pressure data and resistivities of mud filtrates of both wells are also used to perform this study. Lab measurements for the bulk modulus of rock matrix such as quartz and clays are also used as input data.

The methodology of the current study is outlined in three steps: 1) qualitative and quantitative interpretation of wireline logs to derive the physical parameters of reservoir interval such as porosity and permeability, fluids saturation and type, gross and net thickness, shale volume, reservoir temperature and pressure etc. 2) fluid replacement analysis (FRA) to derive seismic velocities (P and S) and densities as a function of natural gas composition and gas/water saturations in the reservoir sands 3) P converted P and S, S converted S and P response, ΔR_{PP}, ΔR_{PS}, ΔR_{SS} and ΔR_{SP} calculations by using the Zoeppritz equations and the derivation of AVO attributes such as intercept and gradient.

The quantitative interpretation of geophysical logs is carried out by using the set of equations given by Ahmed *et al.* (2017b) and various derived logs including shale volume, porosity, water saturation, and lithology are computed and shown in the results section. Thus, the shear log or shear wave velocity was not available for these wells therefore we have used a lithology based equation (Castagna *et al.* 1985). The Castagna's formula ($V_P = 1.16V_S + 1.36$) provides V_S in the wet sandstones and is based on the linear relationship between P (V_P) and S (V_S) wave velocities.

Fluid substitution analysis (also defined as FRA) is an important part of reservoir characterization at exploration and development phases and help to extract the pore fluids type and saturation level from seismic data and borehole sonic data. Various methods have been presented for fluid substitution analysis (Ahmed *et al.* 2018) but Gassmann's formulation (1951) is by far the most extensively used to estimate the seismic velocities variations because of fluid types and saturations in the reservoir rocks at in-situ conditions (Singha and Chatterjee 2017).

Various assumptions have been considered to derive the Gassmann's relation from complex elastic wave theory (EWT) for the poroelastic medium saturated with fluids (liquid/gas) and these assumptions are also undertaken to perform this study. The Gassmann's model of poroelasticity theorizes the rock under study should be macroscopically homogeneous, linear, and isotropic (for rock matrix) and wavelength of seismic waves must be larger than pore/grain size of the reservoir rock. In other words, this relation computes the elastic modulus at low seismic frequencies (Wang 2001). The Gassmann's relation also gives more accurate results for the high porosity rocks with well communicating pores. This model also ignores the interaction between pore fluids and rock matrix to soften or harden the rock skeleton and consider the pore fluid system closed. The well-known Gassmann's formula is

$$K_{sat} = K_{frame} + \frac{\left(1 - \frac{K_{frame}}{K_{matrix}}\right)^2}{\frac{\phi}{K_{fl}} + \frac{(1-\phi)}{K_{matrix}} + \frac{K_{frame}}{K^2_{matrix}}} \tag{1a}$$

Here, K_{sat}, K_{frame}, K_{matrix}, and K_{fl} are the bulk modulus of saturated rock, rock skeleton/frame or dry rock, solid rock matrix and the pore fluid (gas/water) and ϕ is the reservoir effective porosity. Gassmann assumed that shear modulus is not affected by reservoir fluids and remains constant and considered the dry shear modulus (μ_{dry}) equivalent to saturated shear modulus (μ_{sat}).

$$\mu_{dry} = \mu_{sat} \tag{1b}$$

The bulk modulus of rock matrix (K_{matrix}) is estimated by using the Voigt-Reuss-Hill (VRH) averaging method (Hill 1952). This method simply averages the upper and lower bounds of Voigt (1910) and Reuss (1929) bounds respectively and estimates the effective elastic moduli in terms of pore space and rock constituents. The mathematical relation of VRH average method is given as

$$K_{matrix} = \frac{1}{2}(K_{Voigt} + K_{\mathrm{Reuss}}) \tag{2a}$$

whereas, Voigt upper (K_{Voigt}) and Reuss lower (K_{Reuss}) bounds are given below

$$K_{Voight} = \sum_{i=1}^{n} V_i K_i \tag{2b}$$

and

$$K_{\mathrm{Reuss}} = \left(\sum_{i=1}^{n} \frac{V_i}{K_i}\right)^{-1} \tag{2c}$$

here, V and K are the volume fractions and modulus of the ith rock constituents.

The effective dry-rock compressibility of the reservoir is estimated by using the porosity based (if ϕ is less than 35 %) relationship of Murphy *et al.* (1993). The best empirical equation is given as

$$K_{frame} = 38.18(1 - 3.39\phi + 1.95\phi^2) \tag{3}$$

Bulk modulus of fluid (gas/water) is calculated by using Wood's relation (1941) which assumes that the binary fluid phases are homogeneously distributed within pore spaces and liquid-gas phases remain unrelaxed or frozen. It is given by the formula as

$$K_{fl} = \left[\sum_{i=1}^{n} \frac{S_i}{K_i} \right]^{-1} \tag{4}$$

where, K_i is the bulk modulus of the each fluid phase, and S_i is the saturation of each fluid phase. The effective porosity is computed by averaging the porosity derived from density and neutron logs as given by by Azzam and Shazly (2012). Different rock and fluids properties used for this study are given in the Table 1.

Since the fluid substitution analysis has been performed at in-situ (PT) conditions, therefore, it is extremely important to measure the temperature and pressure accurately. It is because the temperature and pressure directly affect the fluid properties (Batzle and Wang 1992). Thus we have used the gradient methods to compute the T and P for both reservoirs and the mathematical formulas for the both parameters are given below

$$T = T_{surf} + T_{grad} * D \tag{5a}$$

and

$$P = P_{surf} + P_{grad} * D \tag{5b}$$

here, the subscript surf and grad represent the surface temperature-pressure and temperature-pressure gradients respectively and D donates the in-situ or reservoir depth in kilometers. The numerical values taken for surface temperature and pressure and temperature-pressure gradients are given in the Table 1.

Zoeppritz equations are used to model the effect of fluid saturations on P converted P and S and S converted S and P reflection amplitudes at the top of wet and gas saturated sands. Set of the Zoeppritz equations are given below

$$\begin{pmatrix} \overset{\downarrow\uparrow}{PP} & \overset{\downarrow\uparrow}{SP} & \overset{\uparrow\uparrow}{PP} & \overset{\uparrow\uparrow}{SP} \\ \overset{\downarrow\uparrow}{PS} & \overset{\downarrow\uparrow}{SS} & \overset{\uparrow\uparrow}{PS} & \overset{\uparrow\uparrow}{SS} \\ \overset{\downarrow\downarrow}{PP} & \overset{\downarrow\downarrow}{SP} & \overset{\uparrow\downarrow}{PP} & \overset{\uparrow\downarrow}{SP} \\ \overset{\downarrow\downarrow}{PS} & \overset{\downarrow\downarrow}{SS} & \overset{\uparrow\downarrow}{PS} & \overset{\uparrow\downarrow}{SS} \end{pmatrix} = M^{-1}N \tag{6}$$

In Eq. (6), the first alphabet denotes the kind of incidence wave at reservoir interface and the succeeding alphabet symbolizes the kind of reflected or transmitted wave. The arrow designates the direction of propagation either downward (↓) or upward (↑). M and N matrices are given as

$$M = \begin{pmatrix} -\sin\theta_1 & -\cos\theta_{S1} & \sin\theta_2 & \cos\theta_{S2} \\ \cos\theta_1 & -\sin\theta_{S1} & \cos\theta_2 & -\sin\theta_{S2} \\ 2\rho_1 V_{S1}\sin\theta_{S1}\cos\theta_1 & \rho_1 V_{S1}\left(1-2\sin^2\theta_{S1}\right) & 2\rho_2 V_{S2}\sin\theta_{S2}\cos\theta_2 & \rho_2 V_{S2}\left(1-2\sin^2\theta_{S2}\right) \\ -\rho_1 V_{P1}\left(1-2\sin^2\theta_{S1}\right) & \rho_1 V_{S1}\sin 2\theta_{S1} & \rho_2 V_{P2}\left(1-2\sin^2\theta_{S2}\right) & -\rho_2 V_{S2}\sin 2\theta_{S2} \end{pmatrix} \tag{7}$$

$$N = \begin{pmatrix} \sin\theta_1 & \cos\theta_{S1} & -\sin\theta_2 & -\cos\theta_{S2} \\ \cos\theta_1 & -\sin\theta_{S1} & \cos\theta_2 & -\sin\theta_{S2} \\ 2\rho_1 V_{S1}\sin\theta_{S1}\cos\theta_1 & \rho_1 V_{S1}\left(1-2\sin^2\theta_{S1}\right) & 2\rho_2 V_{S2}\sin\theta_{S2}\cos\theta_2 & \rho_2 V_{S2}\left(1-2\sin^2\theta_{S2}\right) \\ \rho_1 V_{P1}\left(1-2\sin^2\theta_{S1}\right) & -\rho_1 V_{S1}\sin 2\theta_{S1} & -\rho_2 V_{P2}\left(1-2\sin^2\theta_{S2}\right) & \rho_2 V_{S2}\sin 2\theta_{S2} \end{pmatrix} \tag{8}$$

V_P, V_S and ρ are compressional wave velocity, shear velocity and effective density whereas subscript 1 and 2 represent the upper and lower mediums respectively. θ_1 and θ_2 are the angles of incidence for P converted P and S waves while θ_{s1} and θ_{s2} are the angles of incidence for S converted S and P waves respectively. The explicit forms of Eqs. (7)-(8) are presented by Aki and Richards (1980) and are given in the Appendix A.

Table 1 Fluid (liquid/gases) and reservoir rock properties in both cases that are used to perform fluid substitution modeling at in-situ conditions. The moduli of rock forming minerals have taken from Mavko *et al.* (2009)

Parameters	Case I	Case II	Parameters	Case I	Case II
Reservoir temperature (ºC)	51	62	Reservoir pressure (MPa)	24	30
Surface temperature (ºC)	36.5	25	Surface Pressure (atm)	1	1
Temperature gradient (ºC/km)	9.34	12.7	Pressure gradient (MPa/km)	15	10.34
CH_4 density (g/cm^3)	0.1590	0.1890	C_2H_6 density (g/cm^3)	0.3650	0.3606
Specific gravity of CH_4	0.5537	0.5537	CH_4 bulk modulus (GPa)	0.0513	0.0933
Specific gravity of C_2H_6	1.0378	1.0378	C_2H_6 bulk modulus (GPa)	0.1390	0.1847
Specific gravity of C_3H_8	1.5219	1.5219	C_3H_8 bulk modulus (GPa)	0.5939	0.4484
Density of brine (g/cm^3)	1.002	0.975	Modulus of brine (GPa)	2.4990	2.5870
Quartz bulk modulus (GPa)	37	37	Density of quartz (g/cm^3)	2.65	2.65
Clay bulk modulus (GPa)	21	21	Density of clay (g/cm^3)	2.58	2.58

The intercept (A) and gradient (B) are derived from the well-known Aki and Richards (1980) three terms AVO equation that consider the average (V_{Pave}, V_{Save} and ρ_{ave}) and the differences (ΔV_P, ΔV_S and $\Delta\rho$) of upper and lower media. Aki and Richards equation (1980) in terms of intercept, gradient and curvature (C) is given

$$R(\theta) \approx A + B\sin^2\theta + C\sin^2\theta\tan^2\theta \tag{9}$$

and the intercept-gradient formulas are

$$A = R_P = \frac{1}{2}\left(\frac{\Delta V_P}{V_{Pave}} + \frac{\Delta\rho}{\rho_{ave}}\right) \tag{10}$$

$$B = -2\frac{V_{Save}{}^2}{V_{Pave}^2}\frac{\Delta\rho}{\rho_{ave}} + \frac{1}{2}\frac{\Delta V_P}{V_{Pave}} - 4\frac{V_{Save}^2}{V_{Pave}^2}\frac{\Delta V_S}{V_{Save}} \tag{11}$$

4. Results and discussions

Outlined methodology is applied to the well logs and the results are discussed in different sub-sections below.

4.1 Interpretation of wireline logs

Precise measurements of the petrophysical properties concerning to the pore system, fluid distribution within pores and flow characteristics from the wireline logs help to

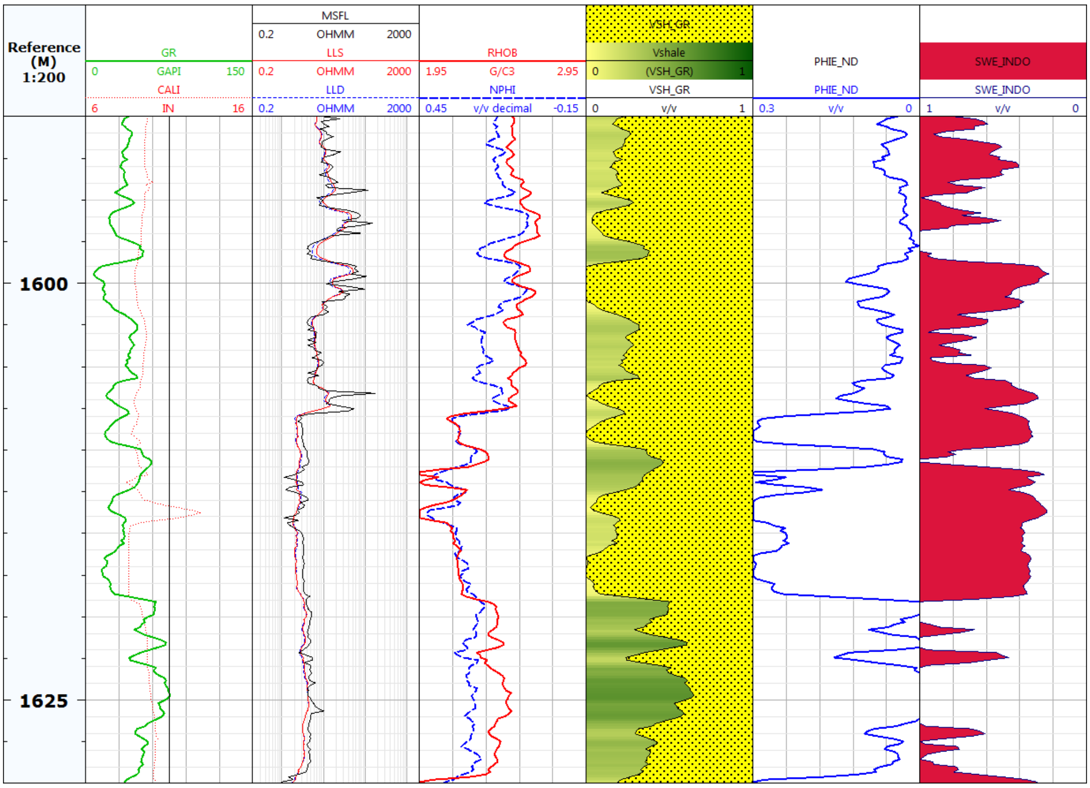

(a)

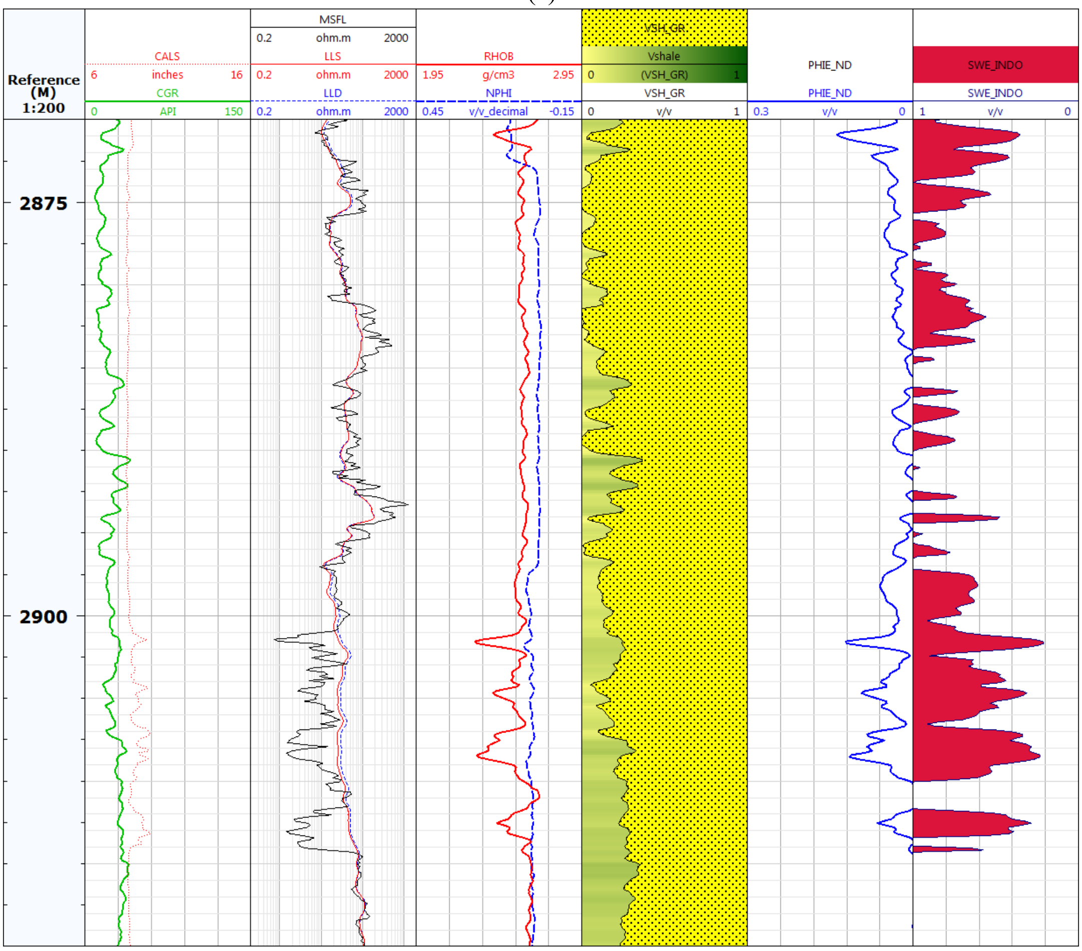

(b)

Fig. 2 Interpretation of wireline logs of both wells (a) case I and (b) case II. It shows the variation of porosity, shale volume, water and hydrocarbons saturations in both case studies

Table 2 Petrophysical properties at net pay thickness levels for both the reservoir intervals (Case I and Case II) are given

	Top (m)	Bottom (m)	Gross Sand (m)	Net Sand (m)	Net to Gross	Shale Volume (frac)	Porosity (frac)	Water Saturation (frac)
Case-I	1590	1630	40	14.26	0.356	0.081	0.26	0.349
Case-II	2870	2920	50	7.375	0.147	0.172	0.07	0.367

evaluate the reservoir rock. It provides the answers of chemical and physical insights of reservoir and fluids characteristics such as bed boundaries, rock type, permeability, pore ratio, fluid saturation identification and pressure etc. that are much needed for fluid substitutions and AVO modeling. Wireline logs interpretation of the Lumshiwal Formation in both wells (case I and case II) is shown in Fig. 2(a) and 2(b). In the first three tracks of Fig. 2, the input measured log curves including gamma ray (GR), caliper (CALI), micro-spherically focused log (MSFL), latero log shallow (LLS), latero log deep (LLD), neutron porosity (NPHI) and density (RHOB) are displayed whereas in the last three tracks, the derived log curves such as porosity, shale volume, matrix volume (shale/sand proportions), water and hydrocarbon saturations (S_W and S_h respectively) are portrayed. In case I, the reservoir rock has shale volume about 20 %, average porosity ~21 %, water saturation ~74 % while on the other hand in case II shale volume is about 9 %, average porosity ~5% and water saturation is about 41 %. However, these numerical values of petrophysical properties are given at gross thickness level. The numerical values at net pay thickness level of shale volume, porosity and water saturation are given in the Table 2. Reservoir rock in case I is situated at shallow depth (1590 m) and therefore has higher porosity and permeability as compare to case II where it is situated at the depth of 2870 m. This decrease in porosity and permeability with increase in depth is due to overburden and compaction of the rock. In Fig. 2, higher hydrocarbon saturation is demarcated at the zone showing neutron-density overlapping and greater porosity. These well logs measurements are further used in Gassmann modeling to analyze AVA responses.

4.2 Gas sand effects on AVO forward modeling: Case I

Seismic signature of pore fluid types and their saturation levels is a key component to decipher the P and S waves reflection coefficients as a function of incident angles/offset: a technique widely used to differentiate the reservoir fluids. P converted P and S and similarly S converted P and S reflection amplitudes are modeled at the top of reservoir sands by assuming different saturation levels of natural gas and brine and shown in Fig. 3. The seismic parameters comprise of velocities and densities at different saturations used to compute these reflection amplitudes (case I) are given in the Table 3. P converted P reflection amplitudes (R_{PP}) as function of angle of incidence at different gas saturations is very sensitive to reservoir fluids type and their saturation levels and displaying

Table 3 The seismic wave velocities and densities for upper shale and reservoir sand (case I) given at different gas-water saturations. These values are used to compute the reflection amplitudes in case I reservoir

	P wave velocity (m/s)	S wave velocity (m/s)	Bulk density (kg/m^3)
Upper Shale	2350.08	853.52	2050
Brine saturated Sandstone	3050.6	1445.9	2210
Gas saturated Sandstone	2816	1521.6	1995.5
50% Gas saturated Sandstone	2916.5	1482.3	2102.7

excellent discrimination between gas saturated sands and wet sands (Fig. 3(a)) as compared to P converted S reflection amplitudes (R_{PS}) shown in Fig. 3(b). In case of R_{PP}, it has higher positive reflection coefficient at zero angle of incidence and decreases towards negative with the increase in angle. However, the rate of change of reflection coefficients is higher and phase reversal occurs after 30° angle in case of gas sand. P converted P reflection is a good indicator at zero angle but it becomes more prominent at higher angles because of more variation in gradient (Fig. 3(a)). On the other hand, P converted S reflection coefficient (Fig. 3(b)) is not a good discriminator as there is a complete overlapping of reflection amplitudes at all different saturations (gas/brine). S converted S reflection coefficient (R_{SS}) can also be a gas sand indicator as it shows comparatively good discrimination in wet and gas sands (Fig. 3(c)). On contrary, S converted P reflection coefficient has poor ability to separate the gas sand as there is almost 100 % overlapping between wet/gas sands (Fig. 3(d)).

In Figs. 4(a)-4(b), ΔR_{PP}, ΔR_{PS}, ΔR_{SS} and ΔR_{SP} are computed by taking the difference between reflection coefficients values at the background (S_w = 1.0) and the target (gas) saturation with respect to incident angles at reservoir interfaces (shale/sand) and plotted. It indicates that the sensitivity to pore fluids increases in all four cases (Fig. 4) as compared to Fig. 3. Both ΔR_{PP} (Fig. 4(a)) and ΔR_{SS} (Fig. 4(c)) have exceptional tendency to separate the not only gas and brine saturated facies but also the partially gas saturated sands. Conversely, both ΔR_{PS} (Fig. 4(b)) and ΔR_{SP} (Fig. 4(d)) do not give good results and strongly overlapping exists in reflectivity curves.

4.3 Gas sand effects on AVO forward modeling: Case II

In case II, reservoir sand has upper contact with the Darsamand Limestone and therefore exhibits different amplitude response as portrayed in Fig. 5. It is because the Darsamand Limestone has high seismic velocities and effective density in contrast with lower sandstone. Reservoir sand has very low porosity and thus almost all the P and S reflection amplitudes (R_{PP}, R_{PS}, R_{SS} and R_{SP}) do not work properly as described in Figs. 5(a)-5(b)). It is because fluids have high impact on seismic and elastic parameters at higher porosities. R_{PP} and R_{SS} have little bit chance of differentiation at lower angles (Fig. 5(a) and 5(c)) and R_{PS} and R_{SP} have separation between gas and wet facies at

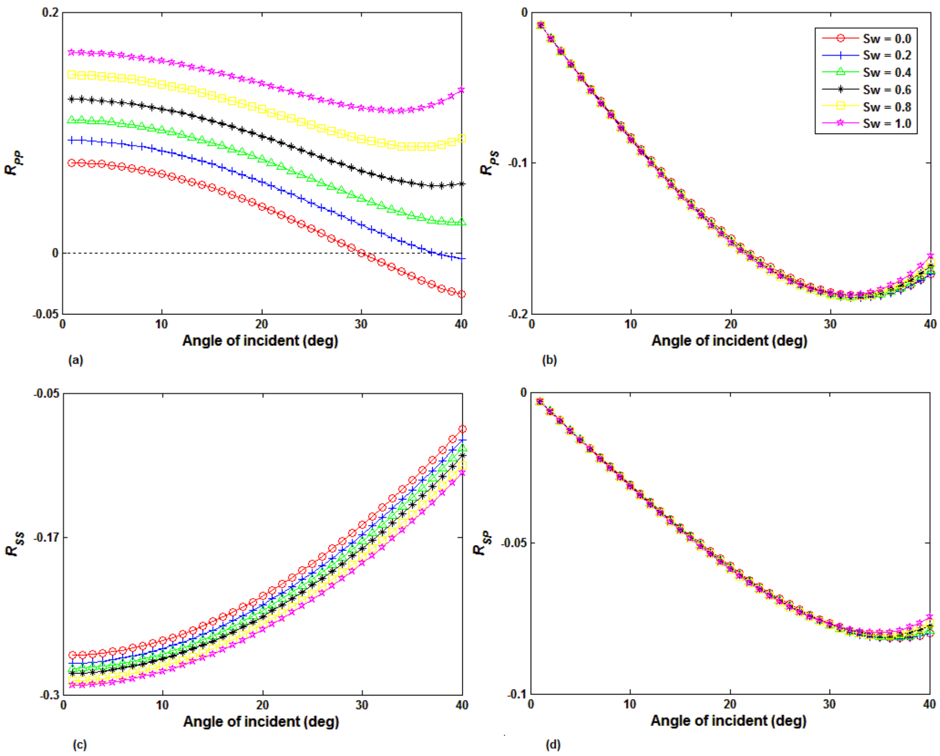

Fig. 3 The effect of natural gas saturations on (a) R_{PP}, (b) R_{PS}, (c) R_{SS} and (d) R_{SP} at the top of reservoir sands is modeled. In case I, gas/wet sands have upper interface with shale of Khadro Formation

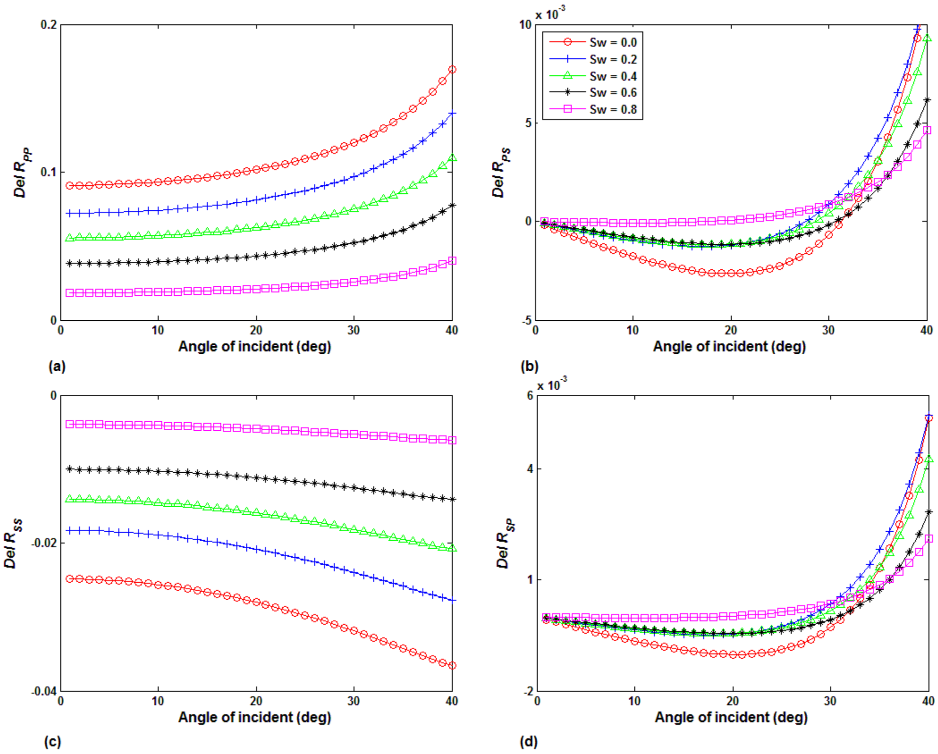

Fig. 4 The effect of gas/brine saturations on (a) ΔR_{PP}, (b) ΔR_{PS}, (c) ΔR_{SS} and (d) ΔR_{SP} at the top of reservoir sands (shale/sand contact) is modeled. ΔR_{PP} and ΔR_{SS} are excellent reservoir fluid indicators and as incident angle increases the gas saturation effects become more pronounced. ΔR_{PS} and ΔR_{SP} are not having better results and reflectivity curves at different saturations overlap on each other

higher incident angles (Fig. 5(b) and 5(d)).

In Figs. 6(a)-6(b), ΔR_{PP}, ΔR_{PS}, ΔR_{SS} and ΔR_{SP} are calculated at Darsamand Limestone/Lumshiwal Sandstone contact and are crossplotted. From the Fig. 6, it is clear that

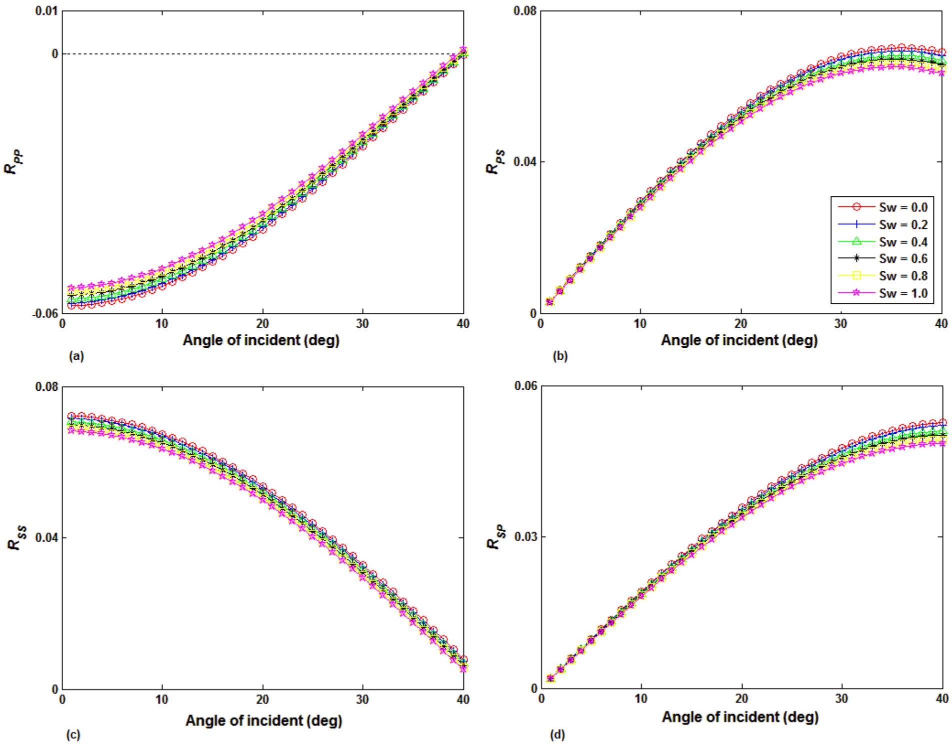

Fig. 5 The effect of gas/water saturations (0%, 20%, 40%, 60%, 80% 100%) on (a) R_{PP}, (b) R_{PS}, (c) R_{SS} and (d) R_{SP} at the top of reservoir sands is modeled. In case II, reservoir sand has upper contact with carbonate rock. All the four reflection amplitude does not provide better results

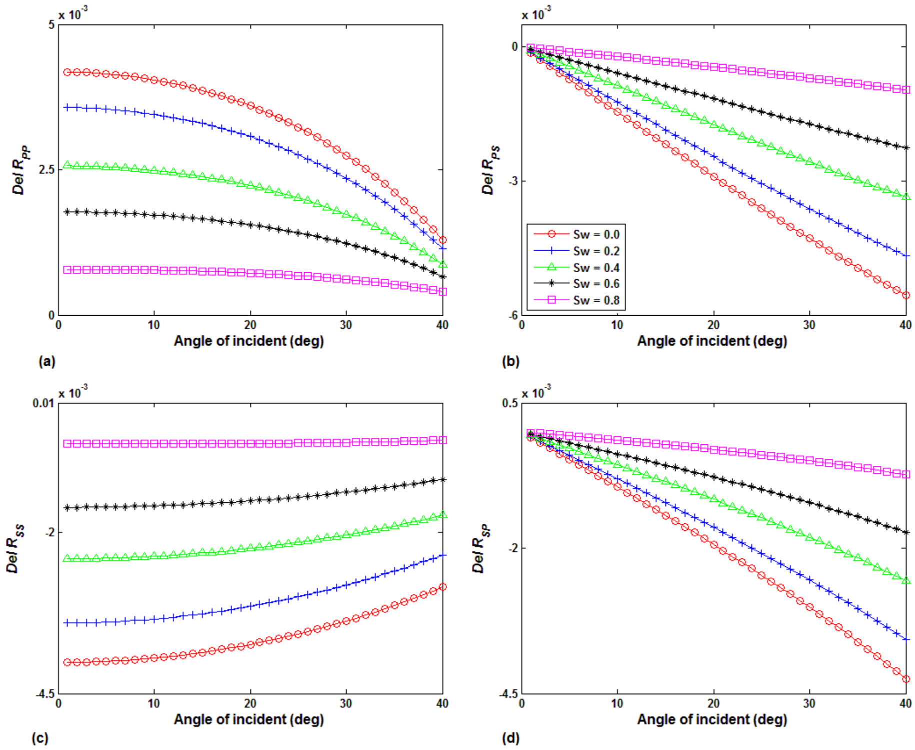

Fig. 6 The effect of gas saturations (0%, 20%, 40%, 60%, 80% 100%) on (a) ΔR_{PP}, (b) ΔR_{PS}, (c) ΔR_{SS} and (d) ΔR_{SP} at the to of reservoir sands is modeled. In case II, reservoir sand has upper contact with carbonate rock. All the four attributes ΔR_{P} ΔR_{PS}, ΔR_{SS} and ΔR_{SP} have very good sensitivity to pore fluids and help to differentiate the gas sand zone very well

all four newly generated AVO indicators work very well especially where the conventional reflectivity curves failed to separate the reservoir fluids and their saturation levels. In case II, reservoir rock has very low porosity (5%) and

Table 4 The seismic wave velocities and densities for upper Limestone and reservoir sand (case II) are given at different gas-water saturations. These values are used to compute the reflection amplitudes in case II reservoir

	P wave velocity (m/s)	S wave velocity (m/s)	Bulk density (kg/m^3)
Upper Limestone	5349.5	3439.2	2720
Brine saturated Sandstone	5203.4	3169.1	2754
Gas saturated Sandstone	4937.4	3110.3	2539
50% Gas saturated Sandstone	5016.8	3152.5	2680

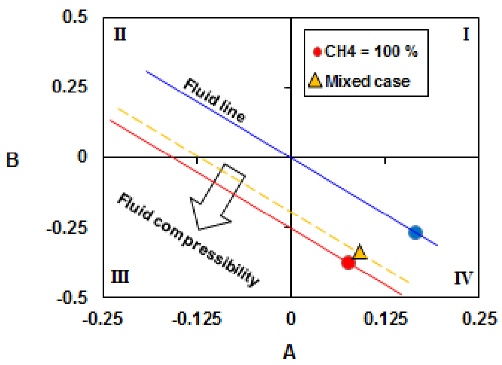

(a) Case I

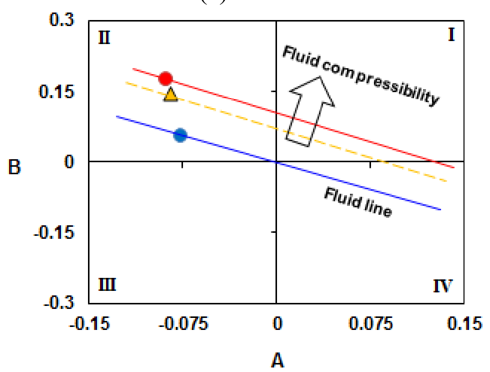

(b) Case II

Fig. 7 Intercept gradient crossplots at the top of both reservoir sands (a) case I and (b) case II. As the fluid compressibility increases (like methane) gas trend lines (red) moves apart from fluid lines (wet trends)

located comparatively at higher depth and thus become difficult to identify gas sand effect on AVA based attributes. However, ΔR_{PP} (Fig. 6(a)), ΔR_{PS} (Fig. 6(b)), ΔR_{SS} (Fig. 6(c)) and ΔR_{SP} (Fig. 6(d)) have good chance in case low porosity. The interesting fact is that both P-P and S-S waves have great tendency to identify gas sand at lower incident angles while P-S and S-P are more sensitive to gas sand at higher incident angles of seismic waves. The seismic parameters comprise of velocities and densities at different saturations used to compute these reflection amplitudes (case II) are given in the Table 4.

4.4 Intercept-gradient crossplotting and effects of natural gas composition

The intercept-gradient crossplotting is extensively used in AVO analysis to detect the gas bearing anomalies. Studies illustrate that changes in in-situ reservoir properties such as pore fluids (gas/liquid) saturation, their compressibility, lithology and pore ratio outcome systematic variations in intercept (A) and gradient (B) spaces. In Fig. 7, intercept-gradient crossplot response at shale/reservoir sand (case I) and Limestone/reservoir sand (case II) is modeled when reservoir sands are saturated with 100% methane (CH_4), mixed gas composition (CH_4, C_2H_6 and C_3H_8 with percentage of 91, 5 and 4 respectively) and 100% brine. Gas response in A-B plot shows clear deviation from fluid line (wet trend). However, in mixed case as ethane (C_2H_6) and propane (C_3H_8) have lower fluid compressibility (inverse of fluid bulk modulus) and trend lines move towards fluid line. In case I, top of gas/wet sands response lie in quadrant IV and for case II, it lies in quadrant II (Fig. 7). Same reservoir sands exhibits different AVO response in A-B plots and follow similar trend like AVO class I gas sand (case I) and class IV gas sand (case II) as reported by Castagna *et al.* (1998). It is because of its upper contact is with different lithologies in both cases.

5. Conclusions

Pore fluids inhomogeneities like saturation levels of fluid phases (liquid/gas), fluid types, composition of natural gas etc. have substantial effect on angle dependent P and S wave reflectivities. However, the sensitivity of each AVA based attributes varies with local rock characteristics and physical properties. Reservoir sand in case I well has high porosity and is at shallow depth therefore both R_{PP} and R_{SS} work better to differentiate gas sands and in low porosity reservoir (case II) strong overlapping in gas-wet sands exists. In case II reservoir, R_{PP}, R_{PS}, R_{SS} and R_{SP} do not distinguish the brine and gas sand facies well. However, the angle based reflectivity curves of ΔR_{PP}, ΔR_{PS}, ΔR_{SS} and ΔR_{SP} are very sensitive to gas saturation and are excellent indicators to identify gas zones even for less porous rocks. Thus, the Intercept-gradient crossplots are better way to identify the gas sand zones. The gas trend lines in A-B plots moves towards fluid lines as the proportion of heavier gases such as ethane and propane increases in the natural gas composition. Same reservoir rock exhibits different AVO class due to upper contact with different sedimentary rock in both cases.

The AVA attributes ΔR_{PP}, ΔR_{PS}, ΔR_{SS} and ΔR_{SP} work well where the conventional AVA indicators fail to identify the gas wells even in the case of low porosity rocks. These attributes can be applied for all the sedimentary sequences (reservoir rocks) of any area. However, the sensitivity of these attributes to the pore fluid type and saturation depend on the local geological conditions and will be different in each case.

Acknowledgements

The authors would like to acknowledge to the Directorate General Petroleum Concessions (DGPC) for providing data to complete the present work. The Institute of Geology, University of the Punjab is also acknowledged for facilitating us in the compilation of this work.

References

Ahmed, N., Badar, M.A., Anwar, M.A., Ahmad, M., Rehman, A.U. and Khalid, P. (2017a), "Application of spreadsheet program in p converted p and s waves amplitudes modeling at geological interface and to identify gas sands", *Geophys. Res. J.*, **4**(1), 11-25.

Ahmed, N., Kausar, T., Khalid, P. and Akram, S. (2018), "Assessment of reservoir rock properties from rock physics modeling and petrophysical analysis of borehole logging data to lessen uncertainty in formation characterization in Ratana Gas Field, northern Potwar, Pakistan", *J. Geol. Soc. India*, **91**(6), 736-742.

Ahmed, N., Khalid, P. Ali, T., Ahmad, S.R. and Akhtar, S. (2016), "Differentiation of pore fluids using amplitude versus offset attributes in clastic reservoirs, Middle Indus Basin, Pakistan", *Arab. J. Sci. Eng.*, **41**(6), 2315-2323.

Ahmed, N., Khalid, P. Shafi, H.M.B. and Connolly, P. (2017b), "DHIs evaluation by combining rock physics simulation and statistical techniques for fluids identification of Cambrian to Cretaceous clastic reservoirs in Pakistan", *Acta Geophys.*, **65**(5), 991-1007.

Ahmed, N., Khalid, P., Ghazi, S. and Anwar, A.W. (2014), "AVO forward modeling and attributes analysis for fluid's identification: A case study", *Acta Geod. Geophys.*, **50**(4), 377-390.

Aki, K. and Richards, P.G. (1980), *Quantitative Seismology: Theory and Methods*, W. H. Freeman and Co., 726.

Azzam, S.S. and Shazly, T.F. (2012), "A comparison between porosity derived from seismic reflection data and that computed from well log data, Al Amal Field, Gulf of Suez, Egypt", *Petrol. Sci. Technol.*, **30**(1), 16-27.

Baig, M.O., Harris, N.B., Ahmed, H. and Baig, M.O.A. (2016), "Controls on reservoir diagenesis in the Lower Goru sandstone formation, Lower Indus Basin, Pakistan", *J. Petrol. Geol.*, **39**(1), 29-48.

Batzle, M.L. and Wang, Z. (1992), "Seismic properties of pore fluids", *Geophysics*, **57**(11), 1396-1408.

Booth, A.D., Emir, E. and Diez, A. (2016), "Approximations to seismic AVA responses: Validity and potential in glaciological applications", *Geophysics*, **81**(1), WA1-W11.

Castagna, J.P., Batzle, M.L. and Eastwood, R.L. (1985), "Relationships between compressional-wave and shear-wave velocities in clastic silicate rocks", *Geophysics*, **50**(4), 571-581.

Castagna, J.P., Swan, H.S. and Foster, D.J. (1998), "Framework for the interpretation of AVO intercept and gradient", *Geophysics*, **63**(3), 948-956.

Chapman, M., Liu, E. and Li, X.Y. (2006), "The influence of fluid-sensitive dispersion and attenuation on AVO analysis", *Geophys. J. Int.*, **167**(1), 89-105.

Gassmann, F. (1951), "Elastic waves through a packing of spheres", *Geophysics*, **16**(4), 673-685.

Golikov, P., Avseth, P., Stovas, A. and Bachrach, R. (2013), "Rock physics interpretation of heterogeneous and anisotropic turbidite reservoirs", *Geophys. Prospect.*, **61**(2), 448-457.

Hedlin, K. (2000), *Pore Space Modulus and Extraction Using AVO,* in *SEG Technical Program Expanded Abstracts 2000*, Proceedings of the 70th Annual International Meeting, Society of Exploration Geophysicists, 170-173.

Hill, R. (1952), "The elastic behavior of a crystalline aggregate", *Proc. Phys. Soc. Sec. A.*, **65**(5), 349-354.

Innanen, K.A. (2011), "Inversion of the seismic AVF/AVA signatures of highly attenuative targets", *Geophysics*, **76**(1), R1-R14.

Kadri, I.B. (1995), *Petroleum Geology of Pakistan*, Pakistan Petroleum Ltd, Karachi, Pakistan.

Kazmi, A.H., and Rana, R.A. (1982), "Tectonic map of Pakistan, bf.", *Geol. Sum. Pakistan*, *Scale*, **1**(2).

Khalid, P., and Ahmed, N. (2016), "Modulus defect, velocity dispersion and attenuation in partially-saturated reservoirs of Jurassic sandstone, Indus Basin, Pakistan", *Stud. Geophys. Geod.*, **60**(1), 112-129.

Khalid, P., Brosta, D. Nichita, D.V. and Blanco, J. (2014), "A modified rock physics model for analysis of seismic signatures of low gas-saturated rocks", *Arab. J. Geosci.*, **7**(8), 3281-3295

Khan, K.A., Anees, A. and Ahmed, N. (2015), "An educational tool for Zoeppritz equations and their various approximations", *Geophys. Res. J.*, **3**(1), 49-54.

Liu, C., Gosh, D.P., Salim, A.M.A. and Chow, W.S. (2019), "A new fluid factor and its application using a deep learning approach", *Geophys. Prospect.*, **67**(1), 140-149.

Mavko, G., Mukerji, T. and Dvorkin, J. (2009), *The Rock Physics Handbook*, Cambridge University Press, Cambridge, U.K.

Murphy, W., Reischer, A. and Hsu, K. (1993), "Modulus decomposition of compressional and shear velocities in sand bodies", *Geophysics*, **58**(2), 227-239.

Narongsirikul, S., Mondol, N.H. and Jahren, J. (2019), "Acoustic and petrophysical properties of mechanically compacted overconsolidated sands: Part 2—Rock physics modelling and applications", *Geophys. Prospect.*, **67**(1), 114-127.

Reuss, A. (1929), "Berechnung der Fließgrenze von Mischkristallen auf Grund der Plastizitätsbedingung für Einkristalle", *Z. Angew. Math. Mech.*, **9**(1), 49-58.

Shuey, R.T. (1985), "A simplification of Zoeppritz equations", *Geophysics*, **50**(4), 609-614.

Silin, D. and Goloshubin, G. (2010), "An asymptotic model of seismic reflection from a permeable layer", *Transp. Porous Med.*, **83**(1), 233-256

Singha, D.K. and Chatterjee, R. (2017), "Rock physics modeling in sand reservoir through well log analysis, Krishna-Godavari basin, India", *Geomech. Eng.*, **13**(1), 99-117.

Smith, G.C. and Gidlow, P.M. (1987), "Weighted stacking for rock property estimation and detection of gas", *Geophys. Prospect.*, **35**(9), 993-1014.

Voigt, W. (1910), "Weiteres zu der Bernoullischen Methode der Bestimmung der optischen Konstanten von Metallen", *Ann. D. Physik*, **338**(14), 833-838.

Wang, Z. (2001), "Fundamentals of seismic rock physics", *Geophysics*, **66**(2), 398-412.

Wood, A.B. (1941), *A Textbook of Sound*, G. Bell and Sons, London, U.K.

Wu, X., Chapman, M., Li, X.Y. and Boston, P. (2014), "Quantitative gas saturation estimation by frequency-dependent amplitude-versus-offset analysis", *Geophys. Prospect.*, **62**(6), 1224-1237.

Xu, D., Wang, Y., Gan, Q. and Tang, J. (2011), "Frequency-dependent seismic reflection coefficient for discriminating gas reservoirs", *J. Geophys. Eng.*, **8**(4), 508-513.

Zhang, S., Chen, S. and Li, H.Y. (2016), "Modeling and analysis of frequency-dependent AVO attributes for fluids saturation prediction", *Proceedings of the 78th EAGE Conference and Exhibition*, Vienna, Austria, May-June.

Zhao, L., Han, D., Yao, Q., Zhou, R. and Yan, F. (2015), "Seismic reflection dispersion due to wave-induced fluid flow in heterogeneous reservoir rocks", *Geophysics*, **80**(3), 221-235.

Zhi, L., Chen, S. and Li, X. (2016), "Amplitude variation with angle inversion using the exact Zoeppritz equations—Theory and methodology", *Geophysics*, **81**(2), N1-N15.

Zhu, F., Gibson Jr, R.L., Watkins, J.S. and Yuh, S.H. (2000), "Distinguishing fizz gas from commercial gas reservoirs using

multicomponent seismic data", *Lead. Edge*, **19**(11), 1238-1245.
Zoeppritz, K. (1919), "Erdbebenwellen VIIIB, on the reflection and propagation of seismic waves", *Göttinger Nachrichten*, **1**, 66-84.

GC

Appendix A

Aki and Richards (1980) presented the explicit form of the Zoeppritz equations (1919) for incident and reflected P and S waves by solving the complex matrices given in the Eqs. (7)-(8). The equations are given below

$$R_{PP}(\theta)=\left[\left(b\frac{\cos\theta_1}{V_{P2}}-c\frac{\cos\theta_2}{V_{P2}}\right)F-\left(a+d\frac{\cos\theta_1}{V_{P1}}\frac{\cos\theta_{S2}}{V_{S2}}\right)Hp^2\right]\Big/D \quad \text{(A-1)}$$

$$R_{PS}(\theta)=\left[-2\frac{\cos\theta_1}{V_{P1}}\left(ab+cd\frac{\cos\theta_2}{V_{P2}}\frac{\cos\theta_{S2}}{V_{S2}}\right)pV_{P1}\right]\Big/(V_{S1}D) \quad \text{(A-2)}$$

$$R_{SS}(\theta)=-\left[\left(b\frac{\cos\theta_{S1}}{V_{S1}}-c\frac{\cos\theta_{S2}}{V_{S1}}\right)E-\left(a+d\frac{\cos\theta_2}{V_{S2}}\frac{\cos\theta_{S1}}{V_{S1}}\right)Gp^2\right]\Big/D \quad \text{(A-3)}$$

$$R_{SP}(\theta)=-2\frac{\cos\theta_{S1}}{V_{S1}}\left(ab+cd\frac{\cos\theta_2}{V_{P2}}\frac{\cos\theta_{S2}}{V_{S2}}\right)pV_{S1}/(V_{P1}D) \quad \text{(A-4)}$$

The constants a, b, c, d, E, F, G, H, D and ray parameter (p) are calculated by the relations

$$a=\rho_2\left(1-2\sin^2\theta_{S2}\right)-\rho_1\left(1-2\sin^2\theta_{S1}\right)$$

$$c=\rho_2\left(1-2\sin^2\theta_{S1}\right)+2\rho_2\sin^2\theta_{S2}$$

$$d=2\left(\rho_2 V_{S2}{}^2-\rho_1 V_{S1}{}^2\right)$$

$$E=b\frac{\cos\theta_1}{V_{P1}}+c\frac{\cos\theta_2}{V_{P2}}$$

$$F=b\frac{\cos\theta_{S1}}{V_{S1}}+c\frac{\cos\theta_{S2}}{V_{S2}}$$

$$G=a-d\frac{\cos\theta_1}{V_{P1}}\frac{\cos\theta_{S2}}{V_{S2}}$$

$$H=a-d\frac{\cos\theta_2}{V_{P2}}\frac{\cos\theta_{S1}}{V_{S1}}$$

$$D=EF+GHp^2$$

$$p=\frac{\cos\theta_1}{V_{P1}}=\frac{\cos\theta_2}{V_{P2}}=\frac{\cos\theta_{S1}}{V_{S1}}=\frac{\cos\theta_{S2}}{V_{S2}}$$